On an application of a generalization of the discrete Fourier transform to short time series

J. Grindlay

Abstract: A generalization of the discrete Fourier transform (DFT) is discussed. This generalization or GDFT provides a smooth interpolation between the points of the DFT. The GDFT of a sinusoidal function in a finite time window is (*a*) described in detail and (*b*) shown to coincide (aside from a simple scaling constant) with the corresponding Fourier transform, provided that certain conditions are satisfied by the sinusoidal parameters. The sinusoidal GDFT is proposed as a tool to investigate, (independently of any Fourier transform connection) the sinusoidal nature of time series. The method is applied successfully to the case of a specific trajectory of the Hénon and Heiles model.

PACS Nos.: 02.30, 05.45

Résumé: Nous analysons une généralisation de la transformée discrète de Fourier (DFT). Cette généralisation, ou GDFT, fournit une interpolation douce entre les points de la DFT. La GDFT d'une fonction sinusoïdale dans une fenêtre finie de temps est (*a*) décrite en détail et (*b*) démontrée coïncider (à l'exception d'une constante d'échelle) avec la transformée de Fourier correspondante, à condition que les paramètres sinusoïdaux satisfassent certaines conditions. Nous proposons la GDFT comme outil de recherche (indépendamment d'une connexion avec une transformée de Fourier) du comportement sinusoïdal des séries temporelles. Nous l'utilisons avec succès dans l'étude d'une trajectoire spécifique du modèle de Hénon et Heiles.

[Traduit par la Rédaction]

1. Introduction

The discrete Fourier transform (DFT) is a widely used tool in the analysis of the frequency response for physical systems [1–4]. In the DFT approach, one samples a continuous stream of data or time series at a finite number of equally spaced times and converts the time sample into a frequency sample — a set of DFT values at equally spaced frequency intervals. This frequency interval is determined solely by the size of the observation time window. In principle, one can achieve a finer sampling frequency mesh by using longer observation times. In practice this is not always possible. There can be physical limitations on the magnitude of the observation time. In such cases, the available DFT sampling grid may be too coarse to distinguish significant features, e.g., resonance peaks in the spectrum.

In this paper, we discuss a generalization of the DFT that avoids the coarse-sampling-grid problem. This generalization or GDFT is applied to the case of a sinusoidal signal in a finite time window and

Received November 16, 2000. Accepted March 26, 2001. Published on the NRC Research Press Web site on July 17, 2001.

J. Grindlay. Physics Department, University of Waterloo, Waterloo, ON N2L 1A5, Canada. FAX: (519)-746-8115 e-mail: john.grindlay2@sympatico.ca

 DOI: 10.1139/cjp-79-5-857

Fig. 1. Sketch of $f(t)$, (2.1).

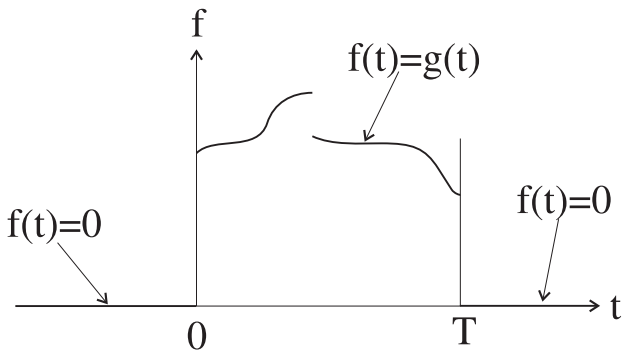

parameter conditions are found for which the GDFT and FT (Fourier transform) are simply related. We also observe that in the sinusoidal case, a very common occurrence in physical situations, the algebraic expressions for the GDFT can be used directly in the analysis of sinusoidal time streams without reference to the FT. That is the GDFT can be used outside any constraints needed to ensure that the GDFT and FT coincide. We illustrate this approach by using it to analyze the dynamical behaviour of a finite section of a trajectory of the simple nonlinear, dynamical system introduced by Hénon and Heiles, [5].

In Sect. 2, we provide a brief background on the Fourier transform. The DFT and its generalization, the GDFT are described in Sect. 3. A number of properties are listed including an equation relating the GDFT and FT. The FT and GDFT are obtained for a sinusoidal time stream in a finite window, Sect. 4. In Sect. 5, the sinusoidal GDFT is used to analyze the time behaviour of a short segment of a trajectory of the Hénon–Heiles model. Section 6 has a short summary of our results.

2. Background

2.1. Fourier transform

Consider a real function of the form, see Fig. 1,

$$\begin{aligned} &f(t) \equiv 0, \qquad T < t \\ &f(t) = g(t), \qquad 0 \leqslant t \leqslant T \\ &f(t) \equiv 0, \qquad 0 < t \end{aligned} \tag{2.1}$$

We may think of f as representing a measurement on a system. The observation begins at $t = 0$ and ends at a later time $t = T$. The system response or behaviour in the interval $[0, T]$ is described by the signal function $g(t)$.

The Fourier transform of a function $f(t)$ is defined to be [6,7]

$$F(\omega) = \frac{1}{\sqrt{2\pi}} \int_{-\infty}^{\infty} f(t) \exp(i\omega t)\, \mathrm{d}t \tag{2.2}$$

where the quantity ω, the frequency, is a real variable. For the function described in (2.1) the transform reduces to

$$F(\omega) = \frac{1}{\sqrt{2\pi}} \int_{0}^{T} g(t) \exp(i\omega t)\, \mathrm{d}t \tag{2.3}$$

We shall assume that $g(t)$ is finite and has a finite number of discontinuities in this period. The transform (2.3) then has the following important properties.

(*i*) Since f is real

$$F(-\omega) = F^*(\omega) \tag{2.4}$$

where the asterisk represents the complex conjugate. Thus, to obtain a complete description of the transform we need only consider positive frequencies.

(*ii*) Since the area under the curve $g(t)$ is finite

$$\lim_{\omega \to \pm\infty} |F(\omega)| = 0 \tag{2.5}$$

As a consequence we can always choose a frequency sufficiently high that $|F(\omega)|$ is as small as we please.

(*iii*) The function f defined in (2.1) is a causal function, (that is $f(t) \equiv 0$ for $t < 0$), and so $F(\omega)$ is a causal transform, [8]. Hence, the real and imaginary parts of the transform are related through the Kramers–Kronig relation, [8,9].

$$F'(\omega) = \frac{1}{\pi} \Pr \int_{-\infty}^{\infty} \frac{F''(z)}{z - \omega} \, \mathrm{d}z, \qquad F''(\omega) = \frac{-1}{\pi} \Pr \int_{-\infty}^{\infty} \frac{F'(z)}{z - \omega} \, \mathrm{d}z \tag{2.6}$$

where F', F'' are the real and imaginary parts of F, respectively, and the integrals are principal values. $F'(\omega)$ and $F''(\omega)$ form a Hilbert transform pair [7].

(*iv*) If f is continuous at the time t the inverse transformation exists and takes the form

$$f(t) = \frac{1}{\sqrt{2\pi}} \int_{-\infty}^{\infty} F(\omega) \exp(-i\omega t) \, \mathrm{d}\omega \tag{2.7}$$

whereas, if f is discontinuous at t, the inverse relationship is

$$\frac{1}{2}[f(t^+) + f(t^-)] = \frac{1}{\sqrt{2\pi}} \int_{-\infty}^{\infty} F(\omega) \exp(-i\omega t) \, \mathrm{d}\omega \tag{2.8}$$

where $f(t^{\pm})$ are the values of f from above and (or) below.

3. Discrete Fourier transform

Let us sample $f(t)$ in the interval $[0, T]$ at the N points

$$t_j = \frac{jT}{N}, \qquad j = 0, 1, 2, ..., N-1 \tag{3.1}$$

This gives a set of N values

$$f_j = f(t_j), \qquad j = 0, 1, 2, ..., N-1 \tag{3.2}$$

Form the N combinations

$$F_s = \frac{1}{N} \sum_{j=0}^{N-1} f_j \exp\left(\frac{2\pi i j s}{N}\right), \qquad s = 0, 1, 2, ..., N-1 \tag{3.3}$$

The complex quantity, F_s, is called the discrete Fourier transform (DFT) of f, [1–4]. Consider the following function:

$$\mathcal{F}(\omega) = \frac{1}{N}\sum_{j=0}^{N-1} f_j \exp\left(\frac{ij\omega T}{N}\right) \tag{3.4}$$

where ω is a continuous, real variable. It follows immediately from (3.3), (3.4) that

$$\mathcal{F}(\omega_s) = F_s \tag{3.5}$$

where $\omega_s = 2\pi s/T$; that is, $\mathcal{F}(\omega)$ provides us with a continuous function passing through all the N values of the DFT. In the Digital Signal Processing literature this function $\mathcal{F}$ is referred to as the "Fourier transform", the "discrete time Fourier transform" [10], or the "discrete Fourier transform" [11]. We prefer to retain the phrase discrete Fourier transform for F_s, (3.3), and to use the alternative nomenclature the "generalized discrete Fourier transform" or GDFT for $\mathcal{F}(\omega)$ in an acknowledgment that the GDFT contains the set of special values F_s, $s = 0, 1, 2, ..., N-1$.

The GDFT, (3.4), has the following properties. Since f is real

$$\mathcal{F}(-\omega) = \mathcal{F}^*(\omega) \tag{3.6}$$

It follows directly from the definition (3.4) that

$$\mathcal{F}(\omega + s\omega_N) = \mathcal{F}(\omega), \qquad s = \pm 1, \pm 2, ... \tag{3.7}$$

with $\omega_N = 2\pi T/N$, i.e., the GDFT is periodic with period ω_N. From (3.6), (3.7) we deduce that

$$\mathcal{F}(\omega) = \mathcal{F}^*(\omega_N - \omega) \tag{3.8}$$

Thus, the $\mathcal{F}(\omega)$ values for ω in the upper half of the frequency range $[0, \omega_N]$, match or repeat those in the lower half range. To avoid this redundancy, we restrict the calculation of the GDFT to the range

$$0 \leqslant \omega \leqslant \frac{\omega_N}{2} \tag{3.9}$$

If $|\mathcal{F}(\omega)|$ has a peak or resonance at Ω, say, then, to ensure that Ω lies in the range (3.9), we must choose a sample number N sufficiently high that $\omega_N/2 > \Omega$ or equivalently

$$N > \frac{\Omega T}{\pi} \tag{3.10}$$

the so-called Nyquist criterion.

The GDFT satisfies the Kramers–Kronig relations (2.6). To prove this, we write from (3.4)

$$\mathrm{Pr}\int_{-\infty}^{\infty} \frac{\mathcal{F}(z)}{(z-\omega)}\,\mathrm{d}z = \frac{1}{N}\sum_{j=0}^{N-1} f_j \,\mathrm{Pr}\int_{-\infty}^{\infty} \frac{\exp(ijzT/N)}{(z-\omega)}\,\mathrm{d}z \tag{3.11}$$

where, as before, "Pr" denotes the principal value operation. With contour integration and Jordan's Lemma applied to the integrals on the right side of this equation, we find

$$\mathrm{Pr}\int_{-\infty}^{\infty} \frac{\mathcal{F}(z)}{(z-\omega)}\,\mathrm{d}z = i\pi\mathcal{F}(\omega) \tag{3.12}$$

The real and imaginary parts of (3.12) yield the Kramers–Kronig relations for the GDFT.

As a final point in this section, we discuss the relationship between the Fourier transform $F(\omega)$, (2.3) and the GDFT $\mathcal{F}(\omega)$, (3.4), see discussion in ref. 10. Given the orthogonality property of the complex exponential, we can invert the definition (3.4) to get

$$f_j = \frac{N}{\omega_N}\int_0^{\omega_N} \mathcal{F}(\omega)\exp\left(\frac{-ij\omega T}{N}\right)\mathrm{d}\omega, \qquad j = 0, 1, ..., N-1 \tag{3.13}$$

From the inverse relation (2.7), (2.8)

$$f_j = \frac{1}{\sqrt{2\pi}}\int_{-\infty}^{\infty} F(\omega)\exp\left(\frac{-ij\omega T}{N}\right)\mathrm{d}\omega, \qquad j = 1, 2, ..., N-1 \tag{3.14}$$

and

$$\frac{f_0}{2} = \frac{1}{\sqrt{2\pi}}\int_{-\infty}^{\infty} F(\omega)\,\mathrm{d}\omega \tag{3.15}$$

We break up the infinite frequency range into segments of width $\omega_N = 2\pi N/T$ and rewrite (3.14) in the form

$$f_j = \frac{1}{\sqrt{2\pi}}\sum_{s=-\infty}^{\infty}\int_{s\omega_N}^{(s+1)\omega_N} F(\omega)\exp\left(\frac{-2\pi ij\omega}{\omega_N}\right)\mathrm{d}\omega, \qquad j = 1, 2, ..., N-1$$

With a change of variable, this expression reduces to

$$f_j = \frac{1}{\sqrt{2\pi}}\sum_{s=-\infty}^{\infty}\int_0^{\omega_N} F(\omega + s\omega_N)\exp\left(\frac{-2\pi ij\omega}{\omega_N}\right)\mathrm{d}\omega, \qquad j = 1, 2, ..., N-1 \tag{3.16}$$

In a similar fashion we can replace (3.15) with

$$\frac{f_0}{2} = \frac{1}{\sqrt{2\pi}}\sum_{s=-\infty}^{\infty}\int_0^{\omega_N} F(\omega + s\omega_N)\,\mathrm{d}\omega \tag{3.17}$$

This set of N equations, (3.16), (3.17), can be put in the form of (3.13) with

$$\mathcal{F}(\omega) = \frac{\sqrt{2\pi}}{T}\sum_{s=-\infty}^{\infty} F(\omega + s\omega_N) + \frac{f_0}{2N} + H(\omega) \tag{3.18}$$

where H is any periodic function satisfying the N conditions

$$\int_0^{\omega_N} H(\omega)\exp\left(\frac{-ij\omega T}{N}\right)\mathrm{d}\omega, \qquad j = 0, 1, ..., N-1 \tag{3.19}$$

We note that the FT, $F(\omega)$, and the GDFT, $\mathcal{F}(\omega)$, are given uniquely by their defining equations, (2.3) and (3.4), respectively. Thus, the arbitrary nature of H is a consequence of the approach used to obtain (3.18), namely, the equating of integrands whose integrals give the same set of sample values, $f_j = f(t_j)$, $j = 0, 1, 2, ..., N-1$. This is the approach described in ref. 10. However, these authors ignore the $f(0^+)$ term and the possibility of the additional periodic term described here by H. As we shall see in the discussion of the special case of a sinusoidal signal function, Sect. 4, both terms do indeed play a role in the relationship between the GDFT and the FT.

4. Single oscillator

Consider the sinusoidal or single oscillator case with signal function

$$g(t) = A\sin(\Omega t + \phi) \tag{4.1}$$

The corresponding Fourier transform, (2.3), is

$$F(\omega) = \frac{-A}{2\sqrt{2\pi}}\left[\exp(i\phi)\frac{[\exp i(\omega+\Omega)T - 1]}{(\omega+\Omega)} - \exp(-i\phi)\frac{[\exp i(\omega-\Omega)T - 1]}{(\omega-\Omega)}\right] \tag{4.2}$$

$|F(\omega)|$ exhibits a resonance at $\omega = \Omega$. When $\Omega T >> 1$, we find $|F(\Omega)| \cong AT/\sqrt{8\pi}$.

For the signal function (4.1), the GDFT is easily shown to be

$$\mathcal{F}(\omega) = \frac{A}{2Ni}\left[\exp(i\phi)\frac{\exp i[(\omega+\Omega)T] - 1}{\exp i[(\omega+\Omega)T/N] - 1} - \exp(-i\phi)\frac{\exp i[(\omega-\Omega)T] - 1}{\exp i[(\omega-\Omega)T/N] - 1}\right] \tag{4.3}$$

As indicated above, the FT and GDFT are related through (3.18), which contains an undetermined function H. Given the sinusoidal results for the FT and GDFT, (4.2) and (4.3), we can solve (3.18) for the corresponding H. We find

$$H(\omega) = -\frac{f(T^-)\exp(i\omega T)}{2N} \tag{4.4}$$

Thus, in the sinusoidal case the GDFT and the FT are related through the equation

$$\mathcal{F}(\omega) = \frac{\sqrt{2\pi}}{T}\left[F(\omega) + \sum_{p=\pm1,\pm2,\ldots}^{\pm\infty} F(\omega + p\omega_N)\right] + \frac{1}{2N}[f(0^+) - f(T^-)\exp(i\omega T)] \tag{4.5}$$

We note that the explicit form of the sinusoidal signal function, (4.1), does not appear in (4.5). This suggests that this equation holds for arbitrary signal function. In particular, the solution for H in (4.4) holds for all $g(t)$. While this is speculation for the GDFT in general, the analogous result for the DFT, namely,

$$F_s = \frac{\sqrt{2\pi}}{T}\left[F(\omega_s) + \sum_{p=\pm1,\pm2,\ldots}^{\pm\infty} F(\omega_s + p\omega_N)\right] + \frac{1}{2N}[f(0^+) - f(T^-)] \tag{4.6}$$

holds for all signal functions, see the Appendix.

It is clear from the discussion in the previous paragraph, that, in general, there is no simple relation between the sinusoidal $\mathcal{F}(\omega)$ and the value of the sinusoidal FT, F at ω. However, for certain restricted ranges of parameters a simple relation exists. For example if

$$N >> 1, \qquad |\omega - \Omega|T << N, \qquad |\omega - \Omega| << \omega + \Omega \tag{4.7}$$

then

$$\mathcal{F}(\omega) \cong \frac{\sqrt{2\pi}}{T}F(\omega) \cong \frac{A}{2T}\exp(-i\phi)\frac{\exp[i(\omega-\Omega)T] - 1}{(\omega-\Omega)} \tag{4.8}$$

Thus, under the conditions displayed in (4.7), the terms described by (*a*) the sum over p and (*b*) the quantities $f(0^+)$, $f(T^-)$ on the right side of (4.5) contribute negligibly to the sinusoidal GDFT.

In the previous paragraph, we were concerned with conditions under which the GDFT, $\mathcal{F}(\omega)$, could be used to calculate to the scaled FT, $F(\omega)$, of a given sinusoidal time stream in a finite window. Now we describe a different tactic. The simple form of the GDFT for the sinusoidal case, (4.3), presents us with an alternative approach — one which does not hinge on knowing the GDFT — Fourier transform connection. Given a time series, which we suspect is sinusoidal in form, we calculate the GDFT and then attempt to fit the results to the simple expression in (4.3) (or sum of expressions). If successful, we obtain sinusoidal parameters, amplitude, frequency, and phase. Since usually we do not know a priori that the signal is a sum of sinusoidal functions, the justification for this approach must be a postiori, namely, the calculated amplitudes, frequencies, and phases can be used successfully to generate the original signal. The simple harmonic oscillator plays a central role in a wide range of physical systems and so this method has potentially many applications. In the next section, we apply this technique to a well-known model in nonlinear dynamics.

We note that feasibly one could also use DFT values to attempt to fit to a sinusoidal form. However, in the case of short-time windows the DFT frequency sampling is too coarse to be useful. We shall see an example of this in the next section.

5. Application

5.1. Hénon–Heiles model (ref. 5)

The Hénon–Heiles equations of motion are

$$\ddot{x} = -x - 2xy \tag{5.1}$$

$$\ddot{y} = -y - x^2 + y^2 \tag{5.2}$$

where x and y are real functions of time t. These equations describe two simple harmonic oscillators each with fundamental frequency unity and quadratic coupling. There are no known general algebraic solutions to (5.1), (5.2). Our knowledge of the trajectories of this model is largely based on the numerical integration of the differential equations.

The trajectory with initial conditions

$$x = 0, \qquad \dot{x} = \frac{1}{\sqrt{3}}, \qquad y = 0, \qquad \dot{y} = 0 \tag{5.3}$$

has the following properties [12,13,14].

(a) After about 340 model seconds the double precision numerical integration data have become sufficiently contaminated by roundoff and truncation errors that they cannot be used with any confidence.

(b) In the first 200 model seconds the trajectory is Lyapunov unstable with a Lyapunov exponent $\lambda = 0.048$ and the system appears (from the behaviour of the functions $x(t)$, $y(t)$) to be undergoing steady oscillatory motion. In the next 140 model seconds the system is again Lyapunov unstable but with a larger Lyapunov exponent $\lambda = 0.14$. The motion in this period also appears to be steady oscillatory. This trajectory segment provides us with two examples of what appears to be steady, oscillatory data in a time window constrained in size. We now describe the results of an analysis of the first 200 s of data using the GDFT.

The equations of motion (5.1), (5.2) with initial conditions (5.3) were numerically integrated using a Runge–Kutta fourth-order algorithm, [15,16], a time step size of 0.02 and double precision arithmetic. The function $x(t)$ was sampled every 0.5 model seconds within the time interval [0,200], i.e., $T = 200$

Fig. 2. Graph of the frequency dependence of $|\mathcal{F}_x|$, (3.4), generated from the numerical solution $x(t)$ of (5.1), (5.2), with initial conditions (5.3), in a time window $T = 200$ and time sampling number $N = 400$.

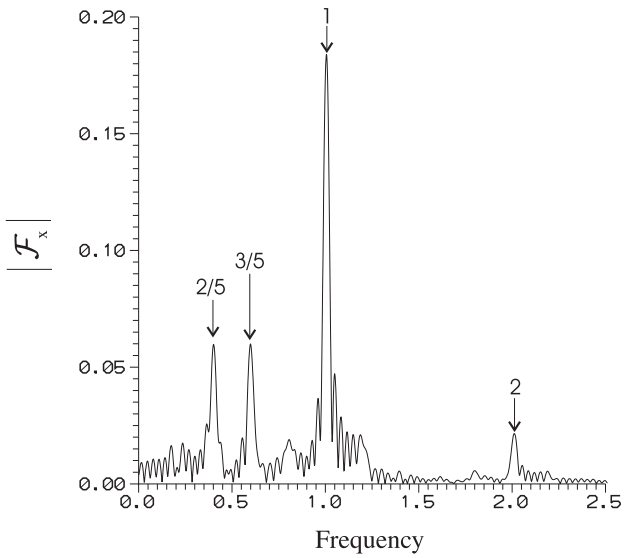

Table 1. Values of the parameters A, Ω, ϕ used in the four oscillator representations for $x(t)$ and $y(t)$, see (5.4).

		x	y
Mode 1	Ω	0.402 ± 0.002	0.403 ± 0.002
	A	0.114 ± 0.004	0.112 ± 0.004
	ϕ	$90° \pm 10°$	$-20° \pm 5°$
Mode 2	Ω	0.600 ± 0.002	0.603 ± 0.002
	A	0.120 ± 0.004	0.128 ± 0.004
	ϕ	$-50° \pm 10°$	$-140° \pm 10°$
Mode 3	Ω	1.005 ± 0.001	1.005 ± 0.001
	A	0.368 ± 0.002	0.368 ± 0.002
	ϕ	$15° \pm 5°$	$110° \pm 10°$
Mode 4	Ω	2.012 ± 0.005	2.010 ± 0.005
	A	0.042 ± 0.004	0.042 ± 0.004
	ϕ	$30° \pm 10°$	$-60° \pm 10°$

and $N = 400$. These data were used to generate the GDFT, (3.4), (denoted by $\mathcal{F}_x(\omega)$) at 50 frequency points between each adjacent pair of DFT frequencies, $[2\pi s/T, 2\pi(s+1)/T]$. The corresponding function $|\mathcal{F}_x|$ is displayed in Fig. 2. This graph shows evidence of four resonances. Thus, as a trial, we write the function x as a sum of four oscillators in the form

$$x(t) = \sum_{j=1}^{4} A_j \sin[\Omega_j t + \phi_j] \tag{5.4}$$

Fig. 3. Graph of the frequency dependence of $\mathrm{Re}\mathcal{F}_x$, (3.4), generated from the numerical solution $x(t)$ of (5.1), (5.2), with initial conditions (5.3), in a time window $T = 200$ and time sampling number $N = 400$. The asterisk points are obtained from the four oscillator representation, (5.5), parameter values in the x-column in Table 1 and time window $T = 200$. The squares are DFT, ($T = 200$, $N = 400$), results for $\mathrm{Re}F_s$, (3.3), from the same $x(t)$. The vertical lines are added for clarity.

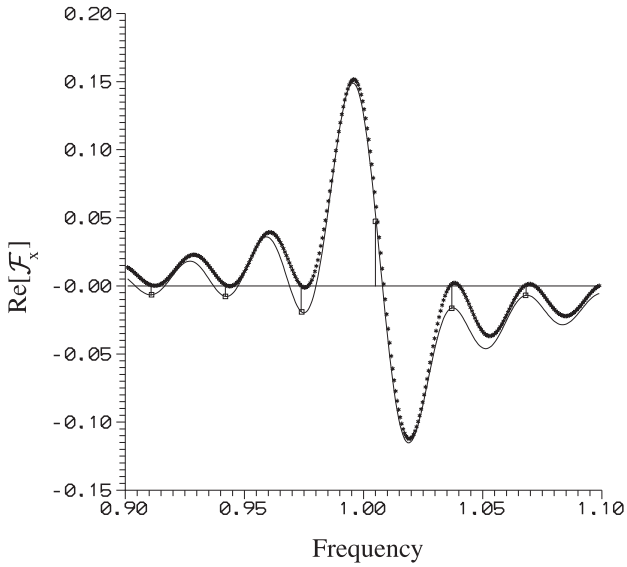

with 12 parameters $A_j,\ \Omega_j,\ \phi_j\ j = 1, 2, 3, 4$.

The corresponding GDFT is then (4.3)

$$\mathcal{F}_s(\omega) = \frac{1}{2Ni}\sum_{j=0}^{n-1}\left[\exp(i\phi_j)\frac{\exp i[(\omega+\Omega_j)T]-1}{\exp i[(\omega+\Omega_j)T/N]-1} - \exp(-i\phi_j)\frac{\exp i[(\omega-\Omega_j)T]-1}{\exp i[(\omega-\Omega_j)T/N]-1}\right] \quad (5.5)$$

The GDFT of the numerical integration for $x(t)$ was fitted to the expression on the right side of (5.5) in the following fashion. From the positions and heights of the peaks in Fig. 2, we determined the four resonant frequencies, Ω_j, and four amplitudes A_j, $j = 1, 2, 3, 4$, see the x-column in Table 1. We then chose the phases to best fit the calculated functions $\mathrm{Re}\mathcal{F}_x(\omega)$ and $\mathrm{Im}\mathcal{F}_x(\omega)$, (5.5), near the resonances. The fit near the fundamental frequency is shown in Figs. 3 and 4. The full curve is the GDFT for $x(t)$ and the asterisks are generated by the function in (5.5) with the parameters in the x-column in Table 1 and window size $T = 200$. We also show the DFT for $x(t)$ in these two figures — squares, with attached vertical lines for clarity. It is clear from Figs. 3 and 4 that the DFT fails to provide a satisfactory description of the fundamental resonance — compare the small number of DFT points, the squares, with the large number of GDFT points, the asterisks. Similar graphs for the other three resonances show similar results. As a final check on the GDFT we used the parameters A_j, Ω_j, ϕ_j in the x column of Table 1 and the representation in (5.5) to generate a set of $x(t)$ values. These are shown as asterisks in Fig. 5. The full curve is the numerical integration data. As a measure of the fit of the four oscillator representation, (5.5), we use the root mean square χ defined as

$$\chi = \frac{\sqrt{\sum_{j=0}^{N-1}[x(t_j) - x_j^p(t_j)]^2}}{N} \quad (5.6)$$

Fig. 4. Graph of the frequency dependence of $\mathrm{Im}\mathcal{F}_x$, (3.4), generated from the numerical solution $x(t)$ of (5.1), (5.2), with initial conditions (5.3), in a time window $T = 200$ and time sampling number $N = 400$. The asterisk points are obtained from the four oscillator representation, (5.5), parameter values in the x-column in Table 1 and time window $T = 200$. The squares are DFT, ($T = 200$, $N = 400$), results for $\mathrm{Im}F_s$, (3.3), from the same $x(t)$. The vertical lines are added for clarity.

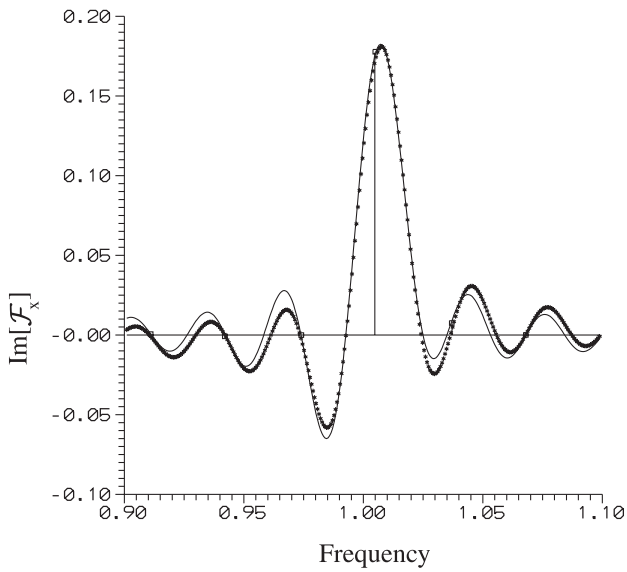

where $x(t_j)$, $x^p(t_j)$ are the value of x from the numerical integration of the equations of motion and the value of x from the sinusoidal representation, (5.4), respectively, both at the time t_j, (3.1). For the data in Fig. 5, we find the RMS result $\chi = 0.005$, indicating that (5.4) gives a satisfactory representation for x in the time interval (0,200). A similar analysis was carried out on the $y(t)$ data. Four resonances are also seen. A similar fitting with four sets of parameters A_i, Ω_i, ϕ_i was carried out successfully, with again a root-mean-square result of 0.005. The parameter values are shown in the y-column of Table 1. The uncertainties shown in Table 1 were estimated from the fitting process.

We note that for both $x(t)$and $y(t)$ the four resonant frequencies are the fundamental $\Omega \cong 1$, the harmonic $\Omega \cong 2$, and two sub-harmonics $\Omega \cong 2/5$, $\Omega \cong 3/5$, each with small anharmonic shifts.

The results of this analysis show that in the first 200 model seconds the trajectory is undergoing steady motion described to a good approximation by a sum of four oscillator functions (5.4).

6. Summary

A generalized discrete Fourier transform, $\mathcal{F}(\omega)$, was defined. This function coincides with the discrete Fourier transform at the DFT sampling frequencies $\omega_n = 2\pi n/T$ and provides a smooth interpolation in the intervals between. Various properties were listed, including periodicity, Nyquist criterion, Kramers–Kronig relations, and a GDFT–FT relation.

An algebraic expression was obtained for the GDFT in the case of a sinusoidal signal function. This expression can be used directly to check for the sinusoidal nature of a given time series. The method consists of fitting a sum of sinusoidal GDFTs to the GDFT of the time series and then using the calculated amplitudes, frequencies, and phases to verify that the original series is indeed represented by a sum of sine functions.

We used this approach to analyze a part of a particular trajectory of the Hénon–Heiles model. The dynamical variables in a specific time window, proved to be well represented by of sums of four

Fig. 5. Graph of the time dependence of $x(t)$ generated from the numerical integration of (5.1), (5.2). The asterisks are the values determined from the four oscillator representation (5.5) and the set of parameter values in the x-column of Table 1.

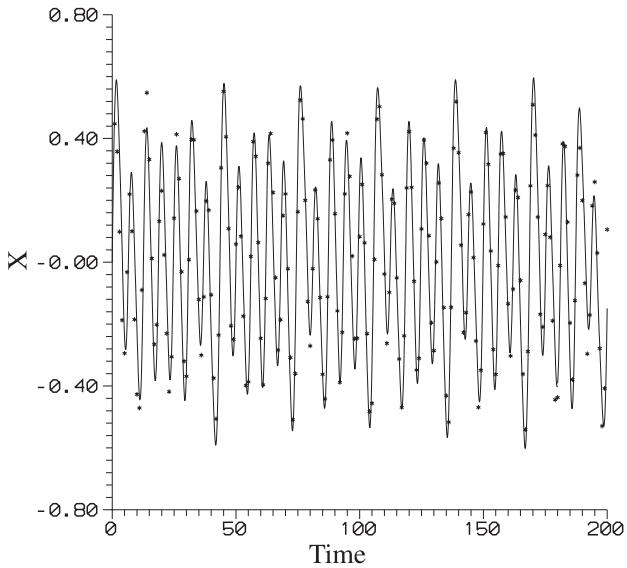

sinusoidal functions.

Acknowledgments

We thank Dr. A.H. Opie and Dr. J. Vanderkooy for a number of stimulating discussions. We also thank the referee for drawing ref. 10 to our attention.

References

1. R.N. Bracewell. The Fourier transform and its applications. McGraw-Hill, New York. 1978.
2. P.M. Duffieux. The Fourier transform and its applications to optics. Wiley, New York. 1983.
3. B.C. Smith. Fundamentals of Fourier transform infrared spectroscopy. CRC Press, Boca Raton. 1996.
4. W.L. Briggs and Van Emden Henson. The DFT: an owner's manual for the discrete Fourier transform. Society for Industrial and Applied Mathematics, Philadelphia. 1995.
5. M. Hénon and C. Heiles. Astron. J. **69**, 73 (1964).
6. I.N. Sneddon. Fourier transforms. McGraw-Hill, New York. 1951.
7. I.N. Sneddon. The use of integral transforms. McGraw-Hill, New York. 1972.
8. E.C. Titchmarsh. Introduction to the theory of Fourier integrals. Clarendon Press. Oxford. 1950.
9. B.W. Roos. Analytic functions and distributions in physics and engineering. Wiley, New York. 1969.
10. A.V. Oppenheim and R.W. Schafer. Digital signal processing. Prentice-Hall, Englewood Cliffs, N.J. 1975.
11. M. Schwartz and L. Shaw. Signal processing. McGraw-Hill, New York. 1975.
12. B.I. Henry and J. Grindlay. Phys. Rev. **E 49**, 2549 (1994).
13. B.I. Henry and J. Grindlay. Can. J. Phys. **75**, 517 (1997).
14. J. Grindlay. Can J. Phys. **77**, 603 (1999).
15. W.H. Press, B.P. Flannery, S.A. Teukolsky, and W.T. Vetterling. Numerical recipes. Cambridge University Press, Cambridge. 1987.
16. J.C. Butcher. The numerical analysis of ordinary differential equations: Runge–Kutta and general linear methods. Wiley, Chichester. 1987.
17. R.V. Churchill. Fourier series and boundary value problems. McGraw-Hill, New York. 1987.

Appendix A:

The Fourier series representation of $f(t) = g(t)$ in the open interval $(0, T)$, [17], is

$$f^F(t) = \sum_{n=-\infty}^{\infty} c_n \exp\left(\frac{-2\pi itn}{T}\right) \tag{A.1}$$

with the Fourier series coefficients defined as

$$c_n = \frac{1}{T}\int_0^T g(t) \exp\left(\frac{2\pi itn}{T}\right) \mathrm{d}t \tag{A.2}$$

At the end points

$$\frac{1}{2}[f(0^+) + f(T^-)] = \sum_{n=-\infty}^{\infty} c_n \tag{A.3}$$

We rewrite this last result in a form to be used below

$$f(0^+) = \sum_{n=-\infty}^{\infty} c_n + \frac{1}{2}[f(0^+) - f(T^-)] \tag{A.4}$$

From a comparison of (A.2) and (2.3) we conclude that

$$c_n = \frac{\sqrt{2\pi}}{T} F\left(\frac{2\pi n}{T}\right) \tag{A.5}$$

The DFT F_n are also related to the Fourier coefficients, the c_n. To prove this, we insert the Fourier series representation for f, (A.1) and (A.4) in the defining equation (3.3)

$$F_s = \frac{1}{N}\sum_{j=0}^{N-1}\left[\sum_{n=-\infty}^{\infty} c_n \exp\left[\left(\frac{-2\pi in}{L}\right)\left(\frac{jL}{N}\right)\right]\right] \exp\left(\frac{2\pi ijs}{N}\right) + \frac{1}{2N}[f(0^+) - f(T^-)] \tag{A.6}$$

Using the identity

$$\begin{aligned} \tfrac{1}{N}\sum_{j=0}^{N-1} \exp\left(\tfrac{2\pi ijs}{N}\right) &= 1, \qquad s = 0, \pm N, \pm 2N, ... \\ &= 0, \qquad \text{otherwise} \end{aligned} \tag{A.7}$$

we can reduce (A.6) to the form

$$F_s = c_s + \sum_{p=\pm1,\pm2,...}^{\pm\infty} c_{s+pN} + \frac{1}{2N}[f(0^+) - f(T^-)] \tag{A.8}$$

When we express the Fourier coefficients in terms of the Fourier transform function, (A.5) we obtain (4.6). The only condition on the validity of (A.8) is that the signal function possesses a Fourier transform.